

## Influence of Extratropical Thermal and Wind Forcings on Equatorial Thermocline in an Ocean GCM\*

HAIJUN YANG

*Department of Atmospheric Science, School of Physics, Peking University, Beijing, China*

ZHENGYU LIU

*Center for Climatic Research and Department of Atmospheric and Oceanic Sciences, University of Wisconsin—Madison, Madison, Wisconsin*

HUI WANG

*National Natural Science Foundation of China, Beijing, China*

(Manuscript received 9 September 2002, in final form 5 June 2003)

### ABSTRACT

The equatorial thermocline variability in the Pacific in response to the extratropical thermal and wind forcings is investigated with an ocean general circulation model [Modular Ocean Model, version 3 (MOM3)]. Sensitivity experiments show that the extratropical wind forcing and thermal forcing contribute equally to the equatorial variability. The wind-induced response is attributed to the off-equatorial wind within 30° of the equator; the thermal-induced response can be traced to higher latitudes. The thermal forcing affects the equator mainly through the equatorward transport of the perturbation temperature by mean subduction flow; the wind forcing affects the equator by changing the strength of meridional overturning circulations. It is also found that the Southern Hemisphere contributes more to the equatorial variability than the Northern Hemisphere under both external forcings.

### 1. Introduction

It has been suggested that the equatorial decadal variability can be modulated by the extratropical oceans through the so-called oceanic bridge (e.g., Gu and Philander 1997; Kleeman et al. 1999). Although some studies emphasize the importance of local forcing in equatorial variability (e.g., Schneider et al. 1999a,b) and illustrate that Ekman pumping in the intertropical convergence zone (ITCZ) tends to block the subduction flow from the ventilation zone in the central North Pacific, the extratropical signal can still reach the equator through either the lower latitude western boundary current (McCreary and Lu 1994; Huang and Liu 1999) or wave dynamics (Lysne et al. 1997). Moreover, more attention has been given to the connection between the equator and Southern Hemisphere (SH). Observations and ocean general circulation models (OGCM) indicate

that the equatorward mass transport from the SH is much larger than that from the Northern Hemisphere (NH; Johnson and McPhaden 1999; Huang and Liu 1999), which may have caused the climate regime shift in 1976/77 in the Pacific (Giese et al. 2002).

In general, two mechanisms that are related to the shallow meridional overturning circulations—the subtropical cells (STCs; McCreary and Lu 1994; Liu et al. 1994) are highlighted in the study of the extratropical contribution to the equatorial decadal variability (Nonaka et al. 2002): the mean advection mechanism, in which the anomalous signal formed in the subtropical ventilation zone is transported to the equator by mean subduction flow (Gu and Philander 1997; Zhang et al. 1998), and the perturbation advection mechanism, by which changes in the STC strength can cause the equatorial temperature to change by varying the amount of equatorward cold water transport (Kleeman et al. 1999; Nonaka et al. 2002). These two mechanisms can work simultaneously to affect the equator. However, recent studies tend to indicate the perturbation advection mechanism as the primary role in equatorial variability. Some model results suggest that the subtropical temperature anomaly cannot significantly affect the equatorial ther-

\* Center for Climatic Research Contribution Number 810.

*Corresponding author address:* Haijun Yang, Department of Atmospheric Science, School of Physics, Peking University, Beijing 100871, China.  
E-mail: hjyang@pku.edu.cn

moocline (Schneider et al. 1999a) due to mixing (Nonaka and Xie 2000) or divergence of the subducted anomalies (Stephens et al. 2001). Conversely, an analysis of historical hydrographic data (McPhaden and Zhang 2002) indicates that a rise in equatorial sea surface temperature (SST) is associated with a slowdown of the meridional overturning circulation in the upper Pacific, consistent with the perturbation advection mechanism.

The extratropical contributions to the equatorial decadal variability have been quantitatively studied by Shin and Liu (2000) and Nonaka et al. (2002). In Shin and Liu, the extratropical thermal forcing in the mid-latitude region can affect the equatorial thermocline very efficiently through the mean advection mechanism. In Nonaka et al., the off-equatorial wind contributed about 50% to the equatorial SST variability through the perturbation advection mechanism. In this paper, the relative contributions of the extratropical thermal and wind forcings to the equatorial thermocline decadal variability are investigated using an OGCM of the Pacific. The study will focus on the following questions: What kind of extratropical forcings contribute more to the equatorial variability? Which forcings are most efficient? What are the relative contributions from the NH and SH?

The OGCM applied here is the Geophysical Fluid Dynamics Laboratory (GFDL) Modular Ocean Model (Pacanowski and Griffies 1999). It is forced with observed SST and wind stress from 1945 to 1992. By designing a set of sensitivity experiments, attempts are made to quantify the response of equatorial thermocline to specified regional extratropical forcings. It is found that the extratropical thermal forcing is more efficient than the wind forcing at disturbing the equatorial thermocline, although both forcings contribute almost equally to the equatorial variability. Under both external forcings, the SH contributes more than the NH to the equatorial variability because of higher efficiency of equatorward penetration of anomalies. This paper is arranged as follows: section 2 introduces the OGCM and the experiments, section 3 compares the control run results with the observations, section 4 discusses results of thermal forcing versus wind forcing, and section 5 summarizes the main results in this paper while providing further discussion.

## 2. Model and experiments

The ocean model used in this paper is the GFDL Modular Ocean Model, version 3 (MOM3; Pacanowski and Griffies 1999). The model domain covers the Pacific from 40°S to 80°N, 100°E to 70°W with a horizontal resolution of 2° in both zonal and meridional directions. There are 32 vertical layers. The model incorporates realistic continents and bottom topography with a maximum depth of 5500 m. A solid boundary is applied at 40°S where model temperature and salinity are restored to Levitus monthly climatology (Levitus 1982). The ver-

TABLE 1. MOM3 experiments. Here, “CR” represents control run, “T” means the global buoyancy run, and “W” means the global wind run. “Clim” means COADS monthly climatology, and “Varying >” represents COADS monthly anomaly applied poleward of latitude indicated.

Expts	Wind	SST	Passive tracer
CR	Varying	Varying	Varying
T	Clim	Varying	Varying
W	Varying	Clim	Varying
T30N	Clim	Varying > 30°N	Varying > 30°N
T15N	Clim	Varying > 15°N	Varying > 15°N
T30S	Clim	Varying > 30°S	Varying > 30°S
T15S	Clim	Varying > 15°S	Varying > 15°S
W30N	Varying > 30°N	Clim	Varying > 30°N
W15N	Varying > 15°N	Clim	Varying > 15°N
W30S	Varying > 30°S	Clim	Varying > 30°S
W15S	Varying > 15°S	Clim	Varying > 15°S

tical viscosity for momentum equations and diffusivity for tracer equations are given as 1.0 and 0.1 cm<sup>2</sup> s<sup>-1</sup>, respectively.

The model is initiated from Levitus (1982) temperature and salinity fields, and spun up for 50 yr with the surface wind stress, SST, and sea surface salinity (SSS) from seasonal climatology of Comprehensive Ocean–Atmosphere Data Set (COADS; da Silva et al. 1994). The SST and SSS forcing are imposed as a surface restoring with a restoring time of 5 days. Such a short restoring time reduces time lags and amplitude errors in the high-frequency component of the model surface tracer fields as pointed out by Pierce (1996), and effectively prevent the model surface tracer fields from drifting away from their long-term climatology.

A control run (CR; Table 1) is performed first by adding the monthly anomalous COADS wind stress and SST from January 1945 to December 1992. Two sensitivity experiments, “wind” run (W) and “buoyancy” run (T), are then performed to study the responses of the equatorial thermocline to different external forcings. The only anomalous forcing is monthly COADS wind stress in the wind run and monthly COADS SST in the buoyancy run. The anomalous forcings are globally applied in these two experiments. The SST in wind run and wind forcing in buoyancy run are restored to their COADS climatology, respectively. Figure 1 shows standard deviations of SST and wind curl for the period from 1945 to 1992. A 5-yr running mean is applied to SST and wind curl to remove interannual variability. Both the SST and wind curl have maximum variability in the ventilation zone of the central North Pacific, suggesting that the central North Pacific is an active source region for the oceanic variability. Observations have shown that subduction starting from this region has substantial influence on the lower latitude thermocline (Deser et al. 1996; Schneider et al. 1999a). In addition, the SST (Fig. 1a) has several submaximum variability centers, manifested in the shadow zone of the eastern North Pacific along the coast of North America, the central equatorial Pacific and the eastern South Pacific along

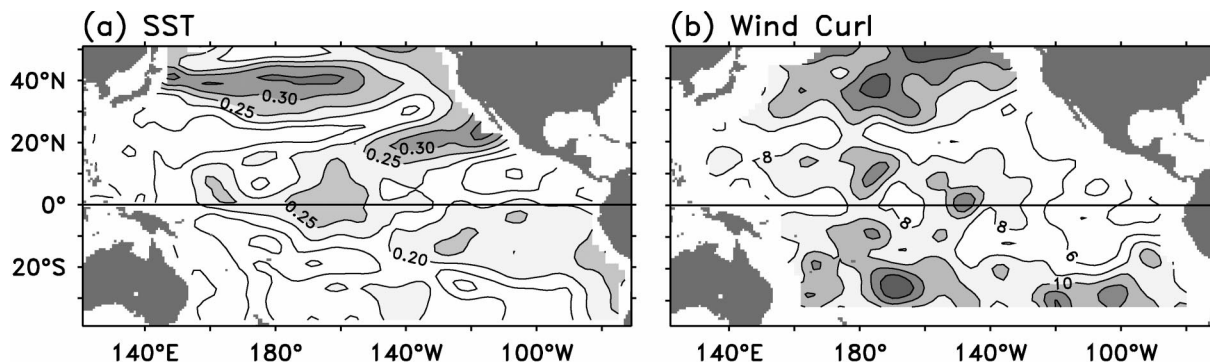


FIG. 1. Standard deviations of the COADS (a) SST and (b) wind stress curl for 1945–92. A 5-yr running mean is applied to SST and wind stress before calculating standard deviation. The contour intervals (CI) are  $0.05^{\circ}\text{C}$  for SST and  $2 \times 10^{-9} \text{ N m}^{-3}$  for wind curl. The contour lines are shaded for SST standard deviation larger than  $0.2^{\circ}\text{C}$  in (a) and for wind curl standard deviation larger than  $8 \times 10^{-9} \text{ N m}^{-3}$  in (b).

the coast of Chile. The wind curl (Fig. 1b) has a submaximum variability center in the central South Pacific, which may be related to the South Pacific subduction source region.

Other sensitivity experiments were performed by imposing localized restoring SST or wind stress anomalies in order to examine the response of the equatorial thermocline to extratropical forcings. There are two groups of experiments (Table 1) to test the latitude of the localized extratropical thermal and wind forcings, respectively. Each group includes four experiments, two of which are strictly for the North Pacific anomalous forcing while the other two are for the South Pacific only, thus testing the remote effect of the North Pacific versus the South Pacific. For example, in the thermal forcing group, T30N (T15N) represents the experiment with anomalous thermal forcing imposed only poleward of  $30^{\circ}\text{N}$  ( $15^{\circ}\text{N}$ ), while in T30S (T15S), the anomalous thermal forcing is imposed poleward of  $30^{\circ}\text{S}$  ( $15^{\circ}\text{S}$ ). In order to compare the dynamics between active and passive tracers, a passive tracer (PT) is also included into all model experiments, which is forced by a surface source that is identical to the anomalous restoring SST. The detailed model configurations are listed in Table 1.

In the following text, a 5-yr running mean was applied for all model outputs in order to focus on the low-frequency variability of the tracer fields.

### 3. Observations and control run

Observations have shown that extratropical decadal signals tend to propagate equatorward along a subduction path, or lines of constant potential vorticity (PV; Fig. 2a) (Schneider et al. 1999a; Stephens et al. 2001). The temperature standard deviation from XBT (1955–94) (White 1995), averaged between the 24 and 26  $\sigma_t$  isopycnal layers, shows large variability along the subduction path (Fig. 3a), as well as in the shadow zone of the eastern North Pacific where PV lines originate at the coast of North America (Fig. 2a). The large standard deviation along the subduction path results primarily from changes in SST (Fig. 1a) within the ventilation zone (Liu and Pedlosky 1994; Schneider et al. 1999a), while the elevated standard deviation in the shadow zone corresponds to Rossby wave responses to changes in Ekman pumping (Liu 1996) and the eastern boundary subduction process (Rothstein et al. 1998).

The model temperature from the control run (Fig. 3b)

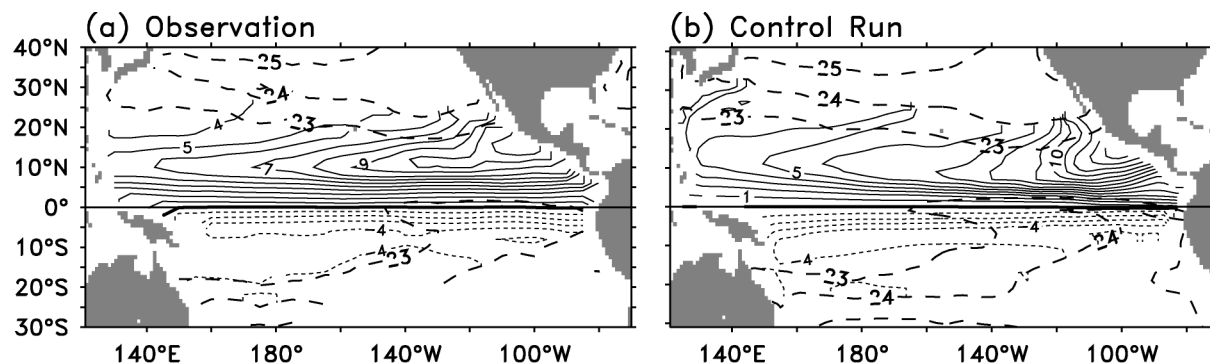


FIG. 2. The climatological mean potential vorticity ( $\text{CI} = 1 \times 10^{-10} \text{ m}^{-1} \text{ s}^{-1}$ ) averaged between 24 and 26  $\sigma_t$  isopycnal layers, derived from (a) XBT and (b) control run, on which the corresponding surface density fields ( $\text{CI} = 1 \text{ kg m}^{-3}$ ) are superposed as thick dashed lines.

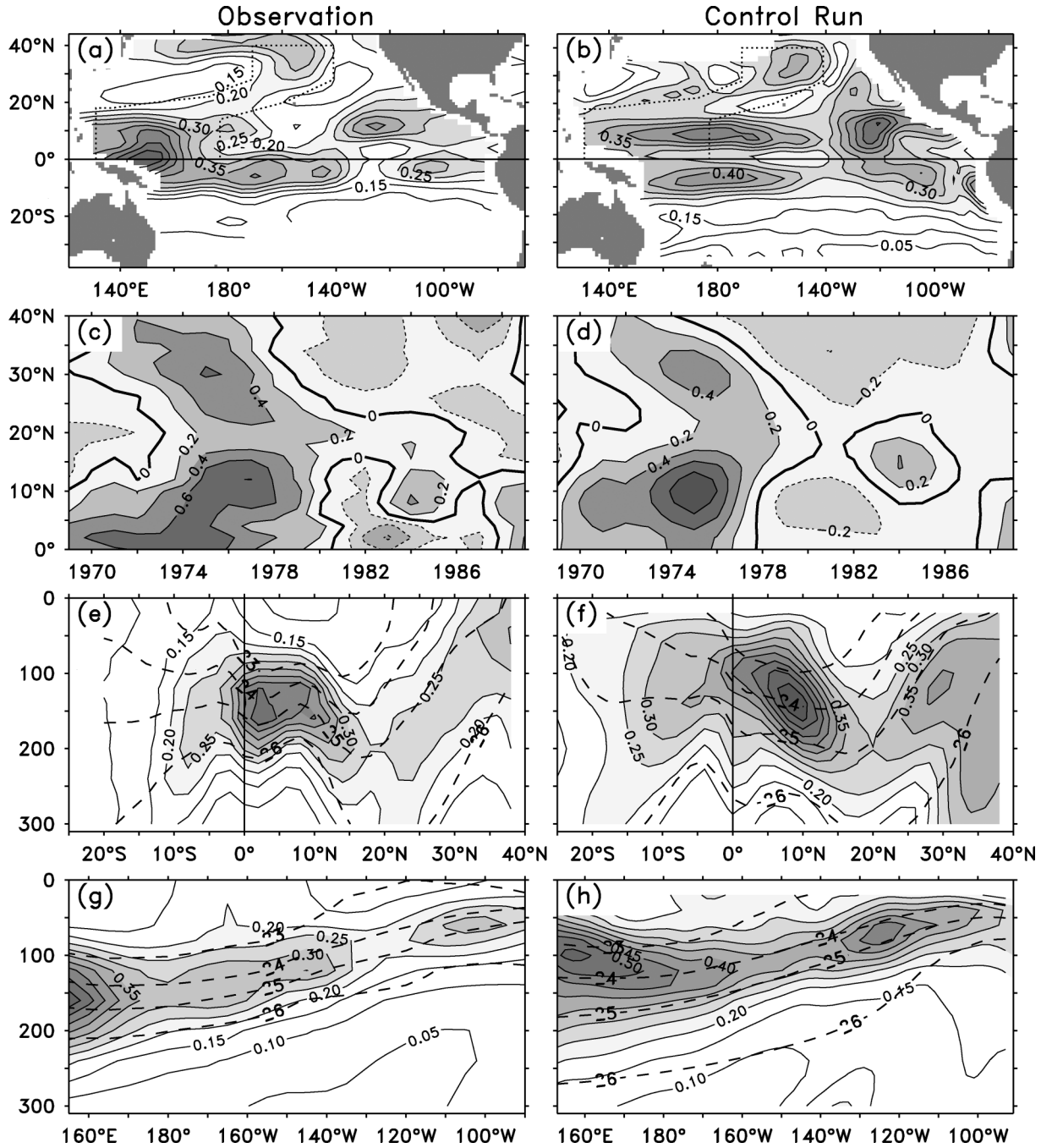


FIG. 3. Standard deviations of the temperature anomalies ( $CI = 0.05^{\circ}C$ ) for (a) XBT and (b) control run averaged between 24 and 26  $\sigma_{\theta}$ . A 5-yr running mean is applied to the temperature anomalies. The contours are shaded for temperature variability larger than  $0.2^{\circ}C$ . The dotted lines in (a) and (b) outline the subduction path along the isopycnal layer in the North Pacific. (c), (d) Time–latitude plots of the temperature anomalies ( $CI = 0.2^{\circ}C$ ) along the subduction path in (a) and (b). (e), (f) Depth–latitude sections of temperature standard deviation ( $CI = 0.05^{\circ}C$ ) along the subduction path, on which the climatological mean isopycnal lines ( $CI = 1 \text{ kg m}^{-3}$ ) are superposed as dashed lines. (g), (h) Depth–longitude plots of temperature standard deviation ( $CI = 0.05^{\circ}C$ ) averaged between  $6^{\circ}S$ – $6^{\circ}N$  with mean isopycnal lines ( $CI = 1 \text{ kg m}^{-3}$ ) superposed as dashed lines.

exhibits a similar pattern and amplitude of the low-frequency variability to the observations (Fig. 3a). The standard deviation values are close to each other in both the ventilation zone and the shadow zone. In the western

Tropics, the model temperature standard deviation has two maximum centers located off equator around  $8^{\circ}$ , which is consistent with the studies of Xie et al. (2000) and Capotondi and Alexander (2001). They concluded

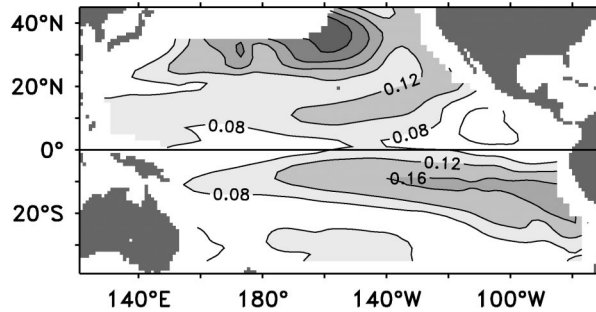


FIG. 4. As in Fig. 3b but for passive tracer ( $CI = 0.04$ ).

that the large temperature variability around  $10^{\circ}\text{N}$  is due to displacements of the thermocline as a whole, associated with baroclinic Rossby waves forced by anomalous Ekman pumping. The mean PV field between  $24$  and  $26 \sigma_t$  from the model (Fig. 2b) also agrees largely with the PV derived from the observation (Fig. 2a), especially the southeastward PV gradients along the subduction pathway, which is critical to the speed of the subduction planetary wave (Stephens et al. 2001).

The latitudinal evolution (Figs. 3c,d) of the subduction temperature anomaly along the subduction pathway (outlined by dotted lines in Figs. 3a,b) shows the propagation of subducted warm subsurface anomalies from the middle to low latitudes through the mid-1970s and subsequent cold anomalies through the mid-1980s. The subduction anomalies appear to be blocked around  $20^{\circ}\text{N}$  and the tropical anomalies seem to be generated locally (Schneider et al. 1999a,b). The model simulation is in good agreement with observations although there are also differences between them. In comparison with the observation (Fig. 3c), the model subduction anomaly (Fig. 3d) is weaker in magnitude in the subtropics and Tropics, and the model warm temperature anomaly seems to propagate faster and the cold temperature anomaly penetrates less southward.

The depth–latitude cross sections (Figs. 3e,f) of the temperature standard deviation along the subduction path show that most of the temperature anomalies originated from the ventilation region propagate equatorward along the isopycnal layer between the  $25$  and  $26 \sigma_t$ . In both the observations and model, the amplitude of temperature variability decays by as much as 30% with its equatorward propagation to around  $20^{\circ}\text{N}$ , which is interpreted as the result of the divergence of group velocity of the subduction planetary wave (Stephens et al. 2001). The maximum temperature variability in the tropical thermocline between the  $23$  and  $26 \sigma_t$  shows a weak connection with the higher-latitude temperature variability, further implying that a local forcing may dominate the tropical Pacific thermocline variability.

The depth–longitude cross sections of the temperature standard deviation along the equator (averaged between  $6^{\circ}\text{S}$  and  $6^{\circ}\text{N}$ ) from observations (Fig. 3g) and the model (Fig. 3h) also show good similarity. The large temper-

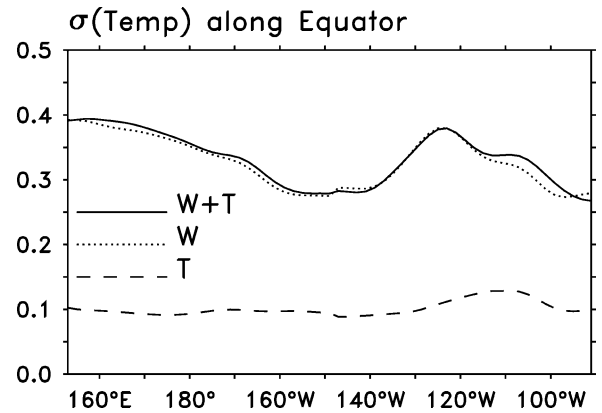


FIG. 5. Standard deviation of temperature averaged between  $23$  and  $26 \sigma_t$  along the equator ( $6^{\circ}\text{S}$ – $6^{\circ}\text{N}$  averaged). The solid, dotted, and dashed lines are for the control run ( $W + T$ ), wind run ( $W$ ), and buoyancy run ( $T$ ), respectively. Note that the large standard deviation in wind run is mainly due to the local Ekman pumping by local wind. The impacts of extratropical wind forcing and thermal forcing on equatorial variability should be comparable, as shown in Figs. 7 and 12.

ature variability between the  $23$  and  $26 \sigma_t$  isopycnals reflects mainly the vertical displacement of the thermocline depth, while the thickness variability of the thermocline is small (figure not shown). The equatorial thermocline anomalous signal tends to extend eastward along the isopycnal and eventually outcrops to the surface in the eastern Pacific. The model reasonably captures these features in nature although it produces a shallower thermocline depth and larger thermocline variability in the western Pacific than in the observations.

The PT in the control run shows large variability in the ventilation zone and shadow zone, as well as in the South Pacific subduction region along the coast of Chile (Fig. 4). These large PT variabilities extend equatorward along subduction pathways in both hemispheres in company with diminishing amplitude. The PT pattern reflects the mean subduction flow since no wave dynamics are involved in the PT redistribution. Figure 4 exhibits a hemispheric asymmetry of the subduction flow. Most equatorward flow in the North Pacific pycnocline flows along constant PV lines to the western boundary where it can easily turn southward. While the analogous flow in the South Pacific originating around  $20^{\circ}\text{S}$ ,  $120^{\circ}\text{W}$  appears to flow northwestward to directly reach the equator (Pierce et al. 2000), and it seems to have a stronger contribution to equatorial tracer variability (Johnson and McPhaden 1999).

The reasonable agreement between the model and observations suggest that the model is reliable to reproduce the major features of the Pacific decadal variability, although Fig. 3 also shows some model–observation discrepancies. In the following text, sensitivity experiments are conducted using this model to further investigate the mechanism of the equatorial thermocline variability.

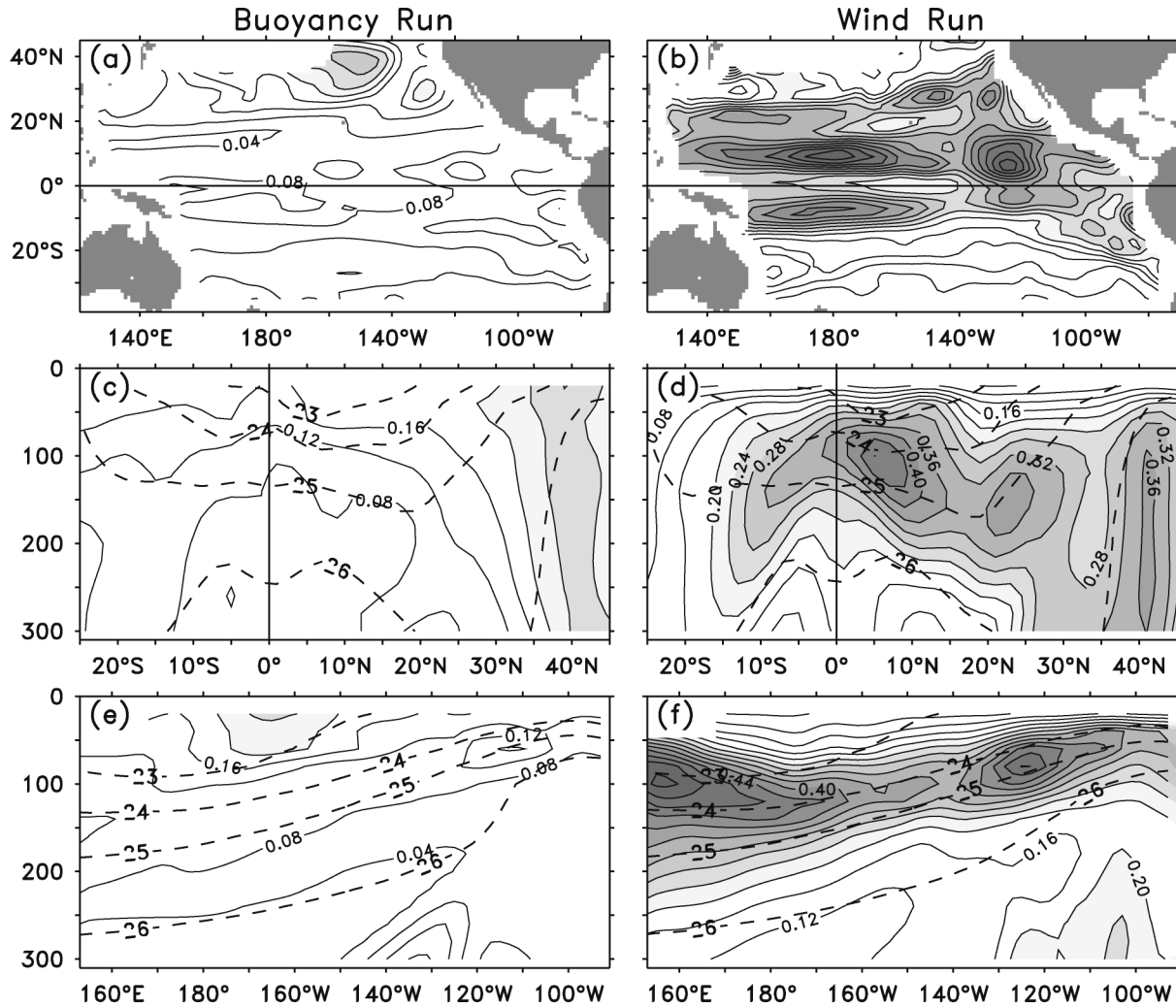


FIG. 6. Standard deviation of temperature ( $CI = 0.04^{\circ}C$ ) averaged between 24 and 26  $\sigma$ , for (a) buoyancy run and (b) wind run. (c), (d) Depth–latitude plots of zonally averaged temperature standard deviation ( $CI = 0.04^{\circ}C$ ) for buoyancy and wind runs, respectively. (e), (f) Depth–longitude plots of temperature standard deviation ( $CI = 0.04^{\circ}C$ ) along the equator. In (c)–(f) the density climatology ( $CI = 1 \text{ kg m}^{-3}$ ) is superposed as dashed lines.

#### 4. Sensitivity experiments

##### a. Thermal forcing versus wind forcing

The amplitudes of the equatorial thermocline variability in response to thermal and wind forcings are significantly different. Here, the results from the global wind and buoyancy runs are discussed first. The wind forcing dominates the equatorial thermocline variability while the thermal forcing only accounts for 30% of the total variability. Figure 5 shows the temperature standard deviation averaged between 23 and 26  $\sigma$ , along the equator for the control run (solid line), buoyancy run (dashed line), and wind run (dotted line). The equatorial temperature variability in the buoyancy run is only  $0.1^{\circ}C$ , in sharp contrast to that of the control run and wind run (about  $0.3^{\circ}$ – $0.4^{\circ}C$ ). Moreover, the thermal forcing produces nearly uniform zonal variability along

the equator, while the wind forcing produces largest variability in the western equatorial Pacific.

The equatorial thermocline response to thermal forcing is the result of two processes: the local response associated with the mixed layer convection and diffusion and the remote response associated with the equatorward subduction of temperature anomalies from higher latitudes. The latter process can also be called the mean advection mechanism ( $\overline{VT'}$ ) (Gu and Philander 1997; Nonaka et al. 2002). This mechanism appears to be the dominant factor in the equatorial thermocline variability in the buoyancy run, while the local effect is negligible. Figure 6a shows that the temperature anomaly subducted from the ventilation zone of the central North Pacific can only reach  $20^{\circ}N$  (Schneider et al. 1999a; Nonaka and Xie 2000). However, the lower-level western boundary Kelvin waves can bring temperature

anomaly signals to the equator (Lysne et al. 1997). There is a clear eastward wedge-shaped wave ridge in the western Pacific along the equator (Fig. 6a), which appears to be the manifestation of eastward equatorial Kelvin waves originating in the higher latitudes of both hemispheres along the western boundary. The local response of the thermocline associated with mixed layer convection and diffusion is very small as shown in Figs. 6c and 6e. Although there is a high standard deviation value of SST in the central equatorial Pacific (Fig. 1a), this surface variability actually has very limited downward penetration and does not even reach the 23.5  $\sigma_t$  isopycnal (Fig. 6e) since the strong mean equatorial upwelling inhibits downward penetration of the surface variability.

In contrast to thermal forcing, the equatorial response to wind forcing is mainly established through three processes: local response associated with Ekman pumping upon the thermocline by equatorial wind, a remote response associated with the baroclinic Rossby wave generated by subtropical wind (Liu and Zhang 1999), and a remote response to changes in the STC strength caused by off-equatorial wind. The last process can also be called the perturbation advection mechanism ( $V'\bar{T}$ ) (Kleeman et al. 1999; Nonaka et al. 2002). Figure 6b shows that northward of 20°N the temperature anomaly does not originate in the ventilation zone but, instead, is related to the eastern boundary subduction process (Rothstein et al. 1998) along the coast of North America and tends to propagate westward by means of the first baroclinic Rossby wave (Liu and Zhang 1999). In the Tropics within 20° of the equator, the large temperature variability (Figs. 6b,d,f) appears to be mainly caused by the local wind (Capotondi and Alexander 2001), as well as changes in the STC strength (Nonaka et al. 2002). These will be further discussed later with more sensitivity experiments to quantify the relative contributions of the local mechanism, the perturbation advection mechanism and Rossby wave mechanism.

The behavior of PT under the wind forcing is very similar to that under thermal forcing. Since the anomalous forcings in these experiments do not affect the mean circulation, the PT variability is thus only determined by the surface source itself. Given the identical surface PT forcings, the PT variabilities thus should be same (figures not shown).

One should bear in mind that the equatorial thermocline response to local wind forcing might be poorly estimated by a pure forced ocean model. The equatorial wind variability may be strongly correlated with the extratropical air–sea system variabilities through atmospheric teleconnections (Pierce et al. 2000). Purely local wind effect cannot be assessed in an OGCM. Consequently, in the following context, only remote responses of the equatorial thermocline to extratropical forcings are examined.

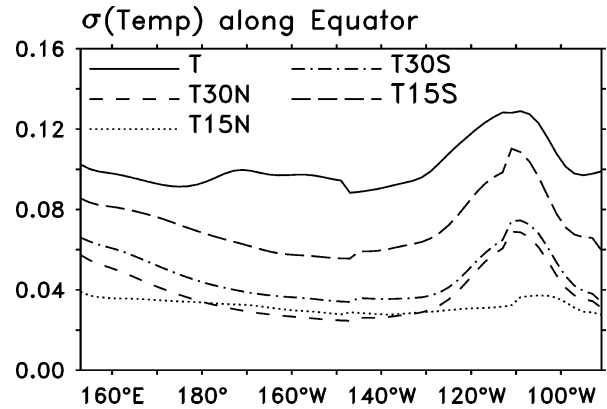


FIG. 7. As in Fig. 5 but for the global buoyancy run (T: solid line), T30N (short dashed line), T15N (dotted line), T30S (dash-dotted line), and T15S (long dashed line).

### b. Extratropical thermal forcing

Four sensitivity experiments (Table 1) were performed to test the equatorial response to extratropical thermal forcing and further examine the relative contributions from the NH versus the SH. A SST anomaly is imposed northward of 30°N (15°N) in T30N (T15N) and southward of 30°S (15°S) in T30S (T15S). First of all, the contribution to the equatorial thermocline variability from the SH is larger than that from the NH (Fig. 7), qualitatively consistent with the study of Giese et al. (2002). In T15S (long-dashed line), the equatorial thermocline variability is about 0.08°C and accounts for 80% of the variability in global buoyancy run (0.1°C). In T30S (dash-dotted line), the equatorial response is about 0.05°C or 50% of the total. The remote response from the NH (short-dashed line for T30N and dotted line for T15N) accounts for no more than 40% of the total. Second, the equatorial variability in T15S is about 0.03°C or 37% more than in T30S, while the variability in T15N is nearly equal to that in T30N in the central equatorial Pacific, and even smaller than that in T30N in the western and eastern equatorial Pacific. One may speculate that the extratropical anomalous forcing should generate a larger equatorial response as the forcing moves closer to the equator. In these experiments, it is true for the SH but not for the NH—a point to be returned later.

The horizontal and vertical structures of temperature variability generated in these four experiments are presented in Fig. 8. In T30N (Fig. 8a), the equatorward subducted anomalous signal originating in the ventilation zone of the central North Pacific seems to be blocked at around 20°N, and there is almost no variability between 5° and 15°N in the western Pacific. However, the equatorial response occurs because of wave dynamics (Lysne et al. 1997; Capotondi and Alexander 2001) and unventilated lower latitude western boundary current (McCreary and Lu 1994). The equatorial Kelvin wave signature along the equatorial thermocline is clear-

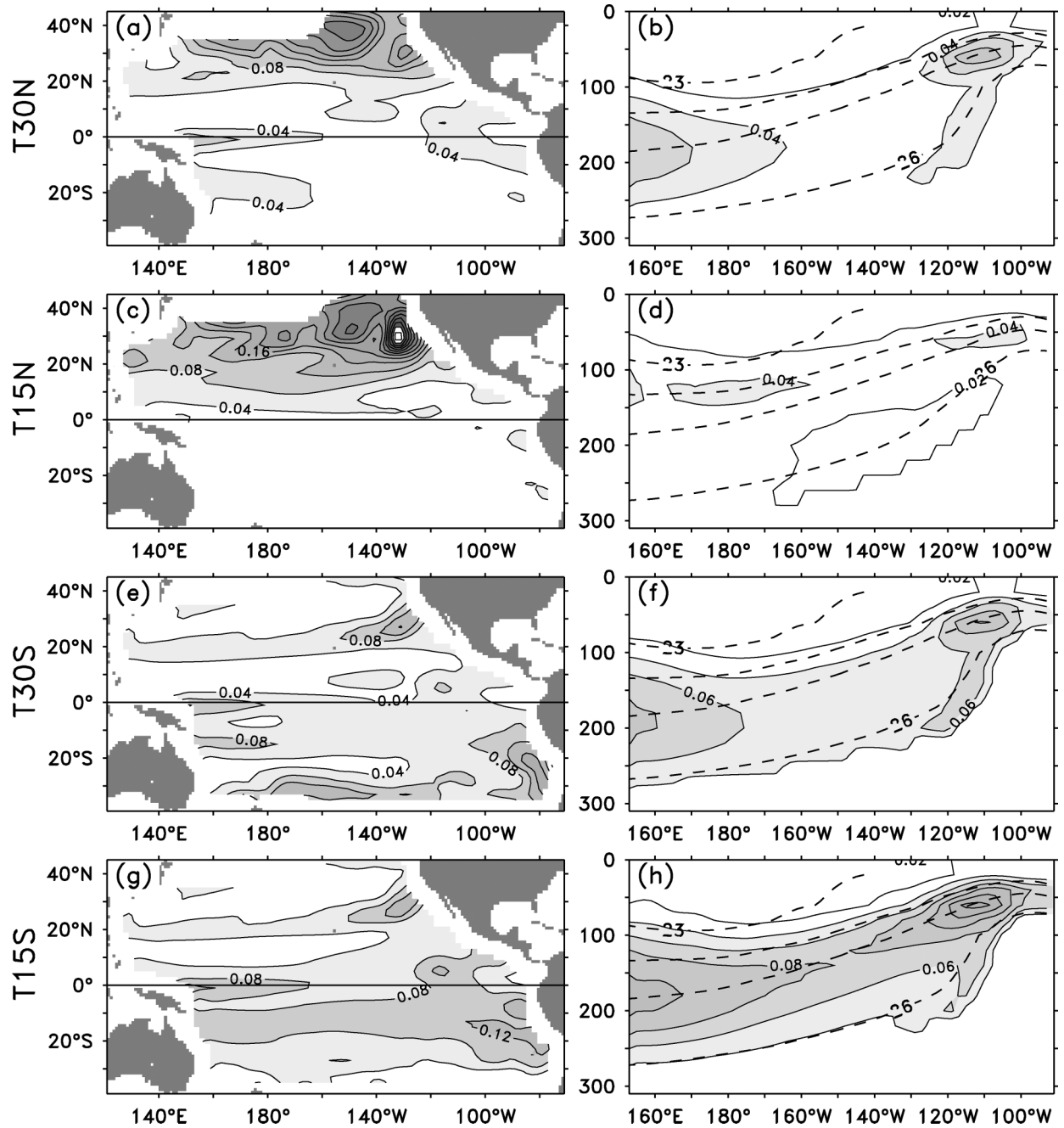


FIG. 8. (left) Standard deviation of temperature ( $CI = 0.04^{\circ}\text{C}$ ) averaged between 24 and 26  $\sigma$ , and (right) depth–longitude plots of the temperature standard deviation ( $CI = 0.02^{\circ}\text{C}$ ) along the equator with model density climatology ( $CI = 1 \text{ kg m}^{-3}$ ) superposed as dashed lines for thermal forcing experiments: (a), (b) T30N; (c), (d) T15N; (e), (f) T30S; and (g), (h) T15S.

ly demonstrated in Figs. 8a,b. The estimated efficiency of equatorward penetration (EEP; Shin and Liu 2000) in T30N is about 20%, given a  $0.04^{\circ}$  and  $0.2^{\circ}\text{C}$  variability in the equatorial thermocline and the North Pacific ventilation zone, respectively. In T15N (Figs. 8c,d), however, the equatorial response is negligible, although the extratropical variability is even larger than that in T30N. There are two extratropical variability centers

located at the ventilation zone and eastern North Pacific along the coast of North America, respectively. These two centers have opposite polarity and tend to cancel each other with equatorward propagation, eventually producing zero net variability at the equator. This cancellation of anomalies has also been documented by Nonaka et al. (2000) and Nonaka and Xie (2000).

Figure 9 presents some clues to understand the small-

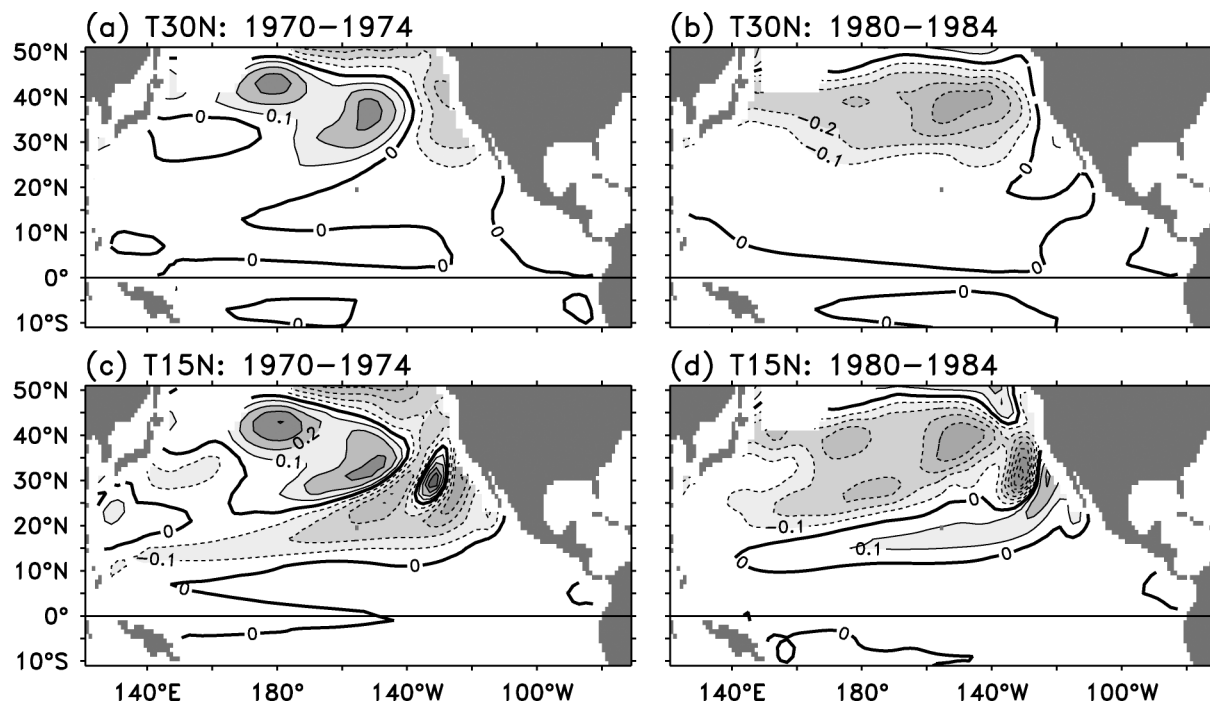


FIG. 9. Mean temperature anomalies ( $CI = 0.1^\circ\text{C}$ ) between 24 and 26  $\sigma$ , averaged for (left) 1970–74 and (right) 1980–84: (a), (b) T30N and (c), (d) T15N.

er equatorial response in T15N than in T30N. Figures 9a,b and 9c,d are two time snapshots of the temperature anomalies averaged for years 1970–74 and 1980–84 between the 24 and 26  $\sigma$ , for T30N and T15N, respectively. The typical pattern of the North Pacific decadal variability is clearly shown in this figure. An anomalous warming in the central North Pacific is usually accompanied by an anomalous cooling along the west coast of North America (Figs. 9a,c) and vice versa (Figs. 9b,d; e.g., Miller et al. 1994; Deser et al. 1996; White and Cayan 1998). In T30N, the amplitude of anomalous warming (cooling) in the central North Pacific during 1970–74 (1980–84) is much stronger than the anomalous cooling (warming) along the west coast of North

America during the same period; therefore, only the central North Pacific variability is accountable for the remote response in the equatorial thermocline. However, in T15N, the anomalous warming (cooling) in the central North Pacific is comparable to the cooling (warming) to the east, while both of them appear to reach the western boundary region at the same time. The right timing to reach the western boundary and comparable amplitude of the two anomalies with opposite sign results in small equatorial thermocline variability.

The SH variability can affect the equatorial thermocline more efficiently than the NH based on experiments T30S (Fig. 8e) and T15S (Fig. 8g). Given a  $0.05^\circ\text{C}$  variability at the equator and  $0.12^\circ\text{C}$  variability in the extratropics in T30S, and corresponding  $0.08^\circ\text{C}$  and  $0.12^\circ\text{C}$  in T15S, the EEPs are about 40% and 66%, respectively. These values are much larger than the estimates in T30N and T15N, suggesting that South Pacific subduction may be more crucial than expected to the equatorial decadal variability (Giese et al. 2002). Furthermore, it seems that the SH variability can cross the equator and further disturb the NH thermocline to some extent (Figs. 8e,g), while the opposite does not happen (Figs. 8a,c). A dynamic connection likely exists between thermocline variabilities in both hemispheres by the eastward equatorial Kelvin waves and westward off-equatorial Rossby wave excited along the western coast of both American continents. Figures 8e and 8g show that, obviously, the anomalous signal in the eastern North Pacific along the coast of North America comes

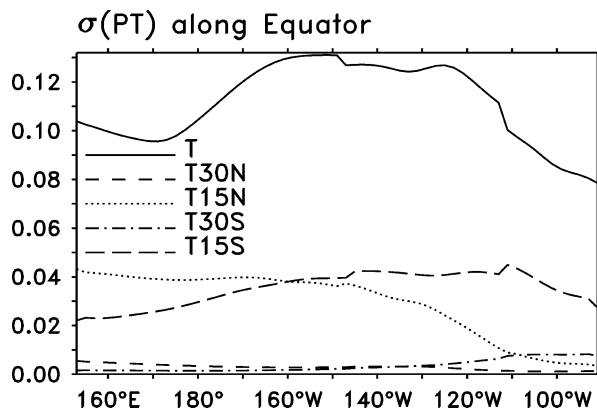


FIG. 10. As in Fig. 7 but for passive tracer.

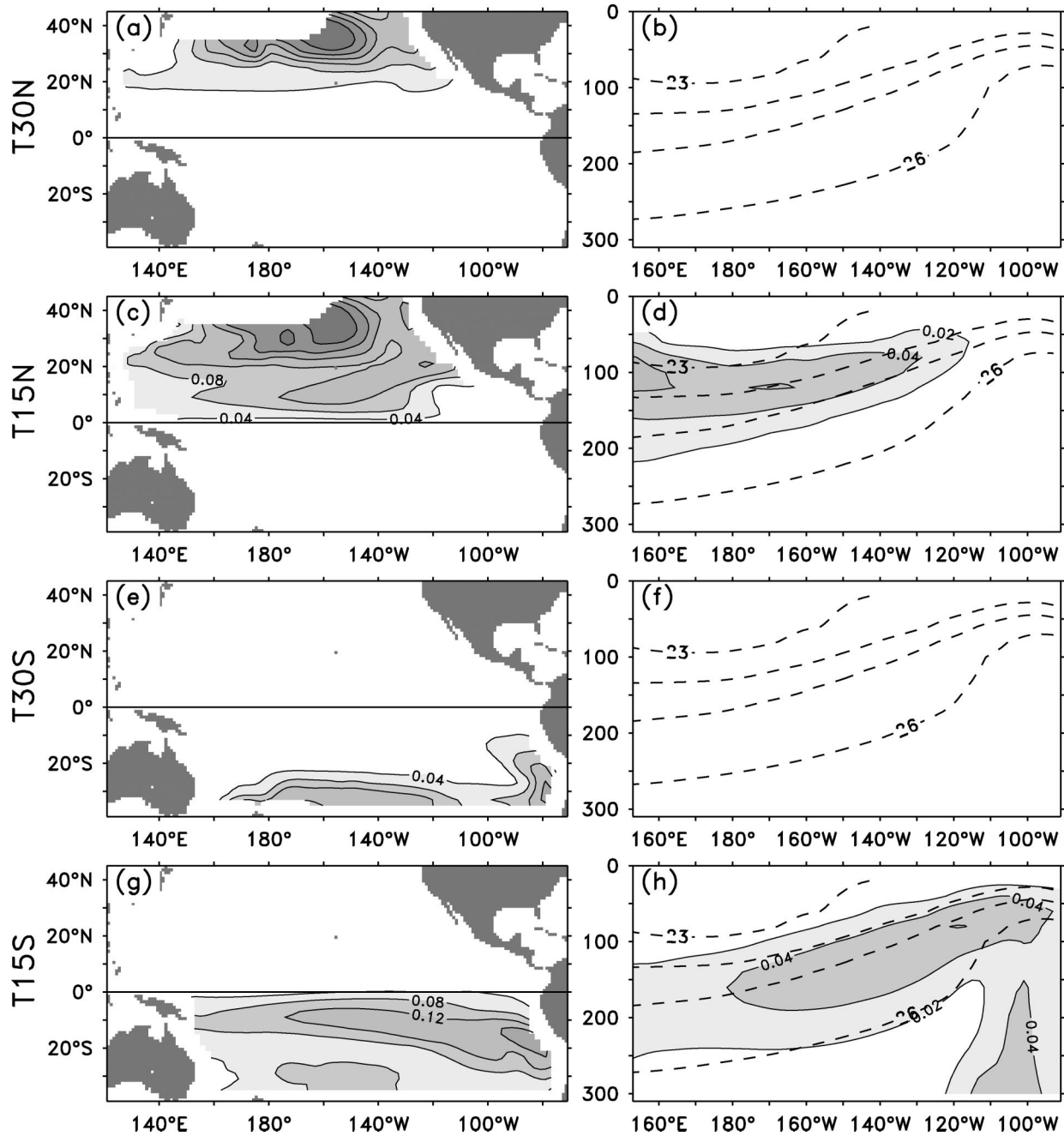


FIG. 11. As in Fig. 8 but for passive tracer.

from the eastern equatorial Pacific by means of a Kelvin wave and further propagates westward along 20°N by means of Rossby waves. This variability is even comparable to that in the SH source regions. The equatorial response caused by the NH variability, however, is too weak to produce a detectable signal in the SH thermocline. In addition, the leakage of the NH waters to the Indian Ocean via Indonesian Throughflow may result in the lack of an NH signature in the SH. The Indonesian Throughflow is also a possible reason why

the SH signals fill the tropical Pacific and spread to higher northern latitudes (McCreary and Lu 2001).

The stronger equatorial thermocline variability in T15S (Fig. 8h) than in T30S (Fig. 8f) occurs because the SH anomalous forcing is closer to the equator in T15S, which can be easily subducted to the equator through the SH interior route without any blocking by the mean current, while the variability in T30S has to first go westward and then turn equatorward. Figure 8g shows that nearly half of the subducted signal originated

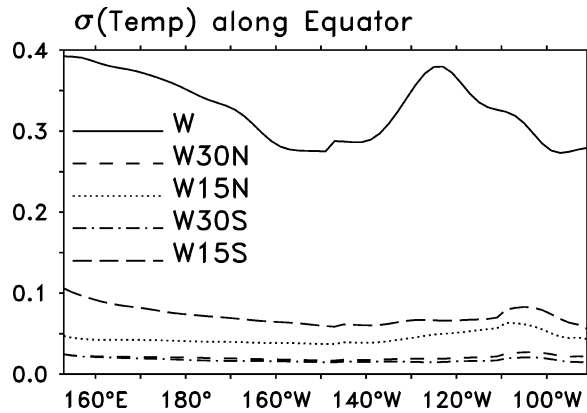


FIG. 12. As in Fig. 7 but for the global wind run (W: solid line), W30N (short dashed line), W15N (dotted line), W30S (dash-dotted line), and W15S (long dashed line).

at 20°S along the coast of Chile directly reaches the eastern equatorial Pacific and even extend westward along the main thermocline (Fig. 8h), forming a high variability center occupying the whole eastern equatorial thermocline.

The PT behavior in these four experiments is very different from temperature. No detectable PT signal in equatorial thermocline is produced in T30N and T30S (Figs. 10, Figs. 11a,b, and 11e,f) because of no wave dynamics involved in PT redistribution. When the surface PT forcing moves closer to the equator, the eastern boundary subduction currents in both hemispheres efficiently carry the anomalous PT signal to the equator through interior routes (Figs. 11c,g), resulting in large PT signal in equatorial main thermocline (Figs. 11d,h). A similar result was also obtained by Nonaka and Xie (2000). The PT EEP is nearly zero in T30N and T30S, but around 15% in T15N and 33% in T15S. One difference between T15N and T15S is that the PT signal in T15N appears to reach the central-western equatorial Pacific first and then go eastward along the isopycnal layer by the equatorial undercurrent (EUC; Fig. 11d), while PT signal in T15S seems to reach the central eastern equatorial Pacific first and is then blocked by the eastward EUC (Fig. 11h).

### c. Extratropical wind forcing

Similar to the extratropical buoyancy runs, four sensitivity experiments (Table 1) were conducted to test the effect of extratropical wind forcing on the equatorial thermocline in which the wind anomalies are imposed northward of 30°N (15°N) in W30N (W15N) and southward of 30°S (15°S) in W30S (W15S), respectively. It is inefficient to disturb the equatorial thermocline by an extratropical wind. In the global wind run, the equatorial thermocline variability is around 0.33°C (Fig. 12); however, it is only about 0.02°C in W30N and W30S and 0.05°–0.07°C in W15N and W15S, respectively. The

extratropical contribution poleward of 30° through the Rossby wave mechanism is only 0.04°C, or 10% of the total, while the contribution through the perturbation advection mechanism is about 0.12°C (0.05°C in W15N plus 0.07°C in W15S) or 36% of the total. This is slightly smaller than, but qualitatively consistent with, the estimates of Nonaka et al. (2002) in which they concluded that the off-equator contribution accounts for about 50% of the equatorial variability.

In the wind runs, the SH also contributes more to the equatorial variability than the NH as shown in W15S (Figs. 13g,h) and W15N (Figs. 13c,d) since the EEP from the SH is higher than that from the NH. It is over 30% in W15S but below 20% in W15N. Figure 13 also indicates that the equatorial variability is predominately caused by an off-equatorial wind within 30° of the equator (Figs. 13c,d,g,h). The subtropical wind poleward of 30° is very inefficient in disturbing the equatorial thermocline (Figs. 13a,b) and also inefficient in generating local variability (Figs. 13e,f). These occur because the strength of STCs is most efficiently changed by the off-equatorial winds in the trade-wind bands (20°–8°S and 8°–25°N), as shown by Nonaka et al. (2002).

### d. STC variability

The extratropical wind generates equatorial thermocline variability mainly through the perturbation advection mechanism, that is, by changing the STC strength. Figure 14a shows the mean meridional overturning streamfunction from the control run. It is clear that the STC contributes significantly to the mass exchange between the equatorial and subtropical region (McCreary and Lu 1994; Liu et al. 1994). The subtropical water subducts in the region of downward Ekman pumping (around 25°N/S) and flows equatorward at depth, then rises to the surface at the equator, and returns poleward by means of Ekman drift under easterly winds. Figure 14b shows the low frequency variability of the divergence of the meridional streamfunction from the contour run (solid line), wind run (dotted line), and buoyancy run (dashed line). Following Nonaka et al. (2002), the divergence of the meridional streamfunction is defined as  $M \equiv \psi'(y_n, z_m) - \psi'(y_s, z_m)$ , where  $\psi'$  is the meridional streamfunction anomaly;  $z_m = 40$  m is the depth of  $M$  maximum;  $y_n = 25^\circ\text{N}$  and  $y_s = 25^\circ\text{S}$  correspond to the region of downward Ekman pumping. In these latitudes, the surface Ekman drift is poleward. Therefore, negative (positive)  $M$  represents a slowdown (speedup) of the STCs.

The nearly identical STC transport between the control run and wind run (Fig. 14b) confirms that the strength of the STC depends only on the wind forcing instead of thermal forcing, which is consistent with McCreary and Lu (1994). The persistent negative  $M$  between 1975 and 1985 is consistent with the equatorial anomalous warming during the same period, in agreement with observations (McPhaden and Zhang 2002)

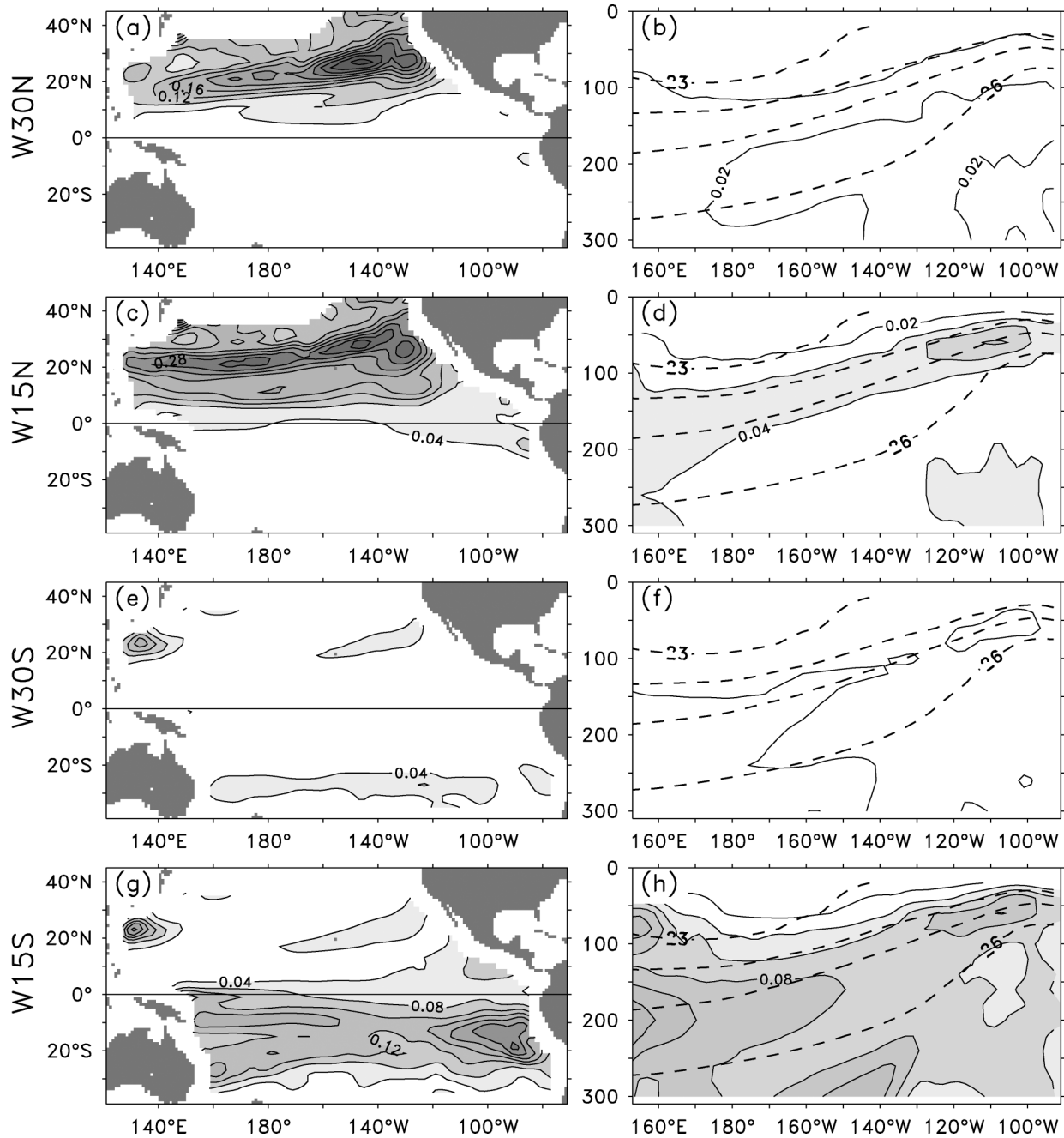


FIG. 13. As in Fig. 8 but for (a), (b) W30N; (c), (d) W15N; (e), (f) W30S; and (g), (h) W15S.

and other model results (Kleeman et al. 1999; Nonaka et al. 2002). The anomalous wind forcings poleward of 30° have no contribution to the equatorial thermocline variability because they have no impact on the STCs strength as shown as short-dashed line (W30N) and dot-dashed line (W30S) in Fig. 14c. The anomalous winds between 15° and 30°N and between 30° and 15°S contribute almost equally to the equatorial variability (dotted line for W15N and long-dashed line for W15S). The

variance contribution is 0.56 Sv (1 Sv  $\equiv 10^6 \text{ m}^3 \text{ s}^{-1}$ ) from the NH and 0.45 Sv from the SH, respectively.

### 5. Conclusions and discussion

The influence of extratropical thermal and wind forcing on equatorial thermocline is studied by an OGCM. Sensitivity experiments were designed to quantify relative contributions of thermal and wind forcings. In

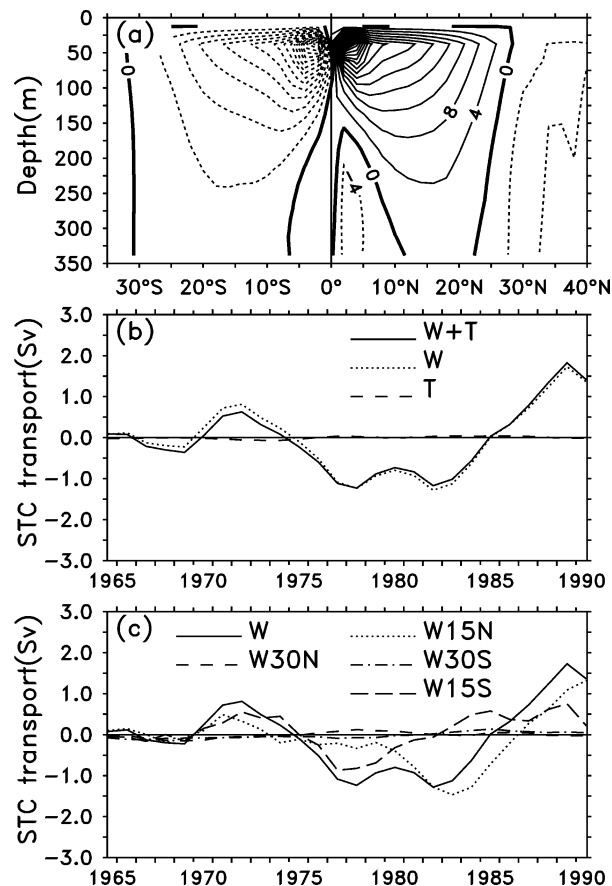


FIG. 14. (a) Mean meridional streamfunction ( $CI = 4 \text{ Sv}$ ) from the control run. (b) Time series of the divergence of the meridional streamfunction anomaly  $M$  for control run ( $W + T$ , solid line), wind run ( $W$ , dotted line), and buoyancy run ( $T$ , dashed line). Five-year running mean is applied to remove interannual variability. (c) Same as (a), but for wind run (solid line),  $W30N$  (short dashed line),  $W15N$  (dotted line),  $W30S$  (dash-dotted line), and  $W15S$  (long dashed line).

terms of absolute contribution, the extratropical wind forcing and thermal forcing contribute equally to the equatorial variability. They account for 36% and 30% of the total equatorial variability, respectively. However, the wind-induced response is attributed to the off-equatorial wind within  $30^\circ$  of the equator, while the thermal-induced response can be traced to higher latitudes. In terms of efficiency, the thermal forcing is more efficient than the wind forcing in disturbing equatorial thermocline. In terms of hemispheric contribution, the SH contributes more than the NH to the equatorial variability in both absolute value and efficiency under both wind and thermal forcings. This is supported by observations (Johnson and McPhaden 1999) and other model studies (Huang and Liu 1999) in which the equatorward mass transport from the SH is much larger than that from the NH.

The mechanisms for the extratropical forcings affecting the equatorial thermocline are different with different external forcings. The thermal forcing affects the

equatorial variability mainly through the mean advection mechanism, while the wind forcing affects the equatorial variability through the perturbation advection mechanism. Both mechanisms are related to the STCs, which play a key role in the mass exchange between the subtropics and Tropics. The first baroclinic Rossby waves generated at mid-high latitudes by anomalous wind forcing contribute little to the equatorial variability.

It is worth noting that the equatorial response in the control run is not equal to the linear combination of that in the wind run and buoyancy run. First of all, the estimation given in this paper is the standard deviation value. Second, one must take into account the nonlinearity that arose from the interaction among different forcings. However, the equatorial response in the global buoyancy run ( $0.1^\circ\text{C}$ ) is very close to the linear superposition of that in  $T15N$  ( $0.03^\circ\text{C}$ ) and that in  $T15S$  ( $0.08^\circ\text{C}$ ), implying a hemispheric symmetric variability with the same polarity (White and Cayan 1998). The total equatorial response ( $0.12^\circ\text{C}$ ) to extratropical wind forcing is estimated by linear superposition of that in  $W15N$  ( $0.05^\circ\text{C}$ ) and that in  $W15S$  ( $0.07^\circ\text{C}$ ). It may not be accurate since the extratropical wind-generated variability could have different signs. One more experiment combining the configurations in  $W15N$  and  $W15S$  should be performed to clarify the above question.

This paper focuses on the remote contribution to the equatorial thermocline from extratropics through the oceanic bridge. The local Ekman pumping seems to contribute at least 50% of the equatorial thermocline variability based on the control run and wind runs. However, the wind forcing used in the OGCM is actually the result of many forms of air-sea interaction, and the tropical wind should have included the extratropical air-sea information so that the tropical SST and thermocline could be strongly modulated by extratropics through the atmospheric bridge (Barnett et al. 1999; Pierce et al. 2000). Therefore, it is unlikely to quantify the “real” local effect in an OGCM, and a coupled ocean-atmosphere general circulation model is thus imperative to separate the local effect from the remote effect and to separate the contribution through oceanic bridge from that through atmospheric bridge.

*Acknowledgments.* The work is supported by NOAA and NSF grants and NSF of China Grant 40306002. Discussions with Drs Q. Zhang and M. Notaro, D.-E. Lee, and Mr. A. Leanna are appreciated. We owe thanks to editor Dr. Eric Firing and, in particular, two anonymous reviewers, who provided invaluable comments on the earlier version of this manuscript.

#### REFERENCES

Barnett, T. P., D. W. Pierce, M. Latif, D. Dommengat, and R. Saravanan, 1999: Interdecadal interactions between the Tropics and

- midlatitudes in the Pacific basin. *Geophys. Res. Lett.*, **26**, 615–618.
- Capotondi, A., and M. A. Alexander, 2001: Rossby waves in the tropical North Pacific and their role in decadal thermocline variability. *J. Phys. Oceanogr.*, **31**, 3496–3515.
- da Silva, A. M., C. C. Young, and S. Levitus, 1994: *Anomalies of Directly Observed Quantities*. Vol. 2, *Atlas of Surface Marine Data 1994*, NOAA Atlas NESDIS 7, 416 pp.
- Deser, C., M. A. Alexander, and M. S. Timlin, 1996: Upper-ocean thermal variations in the North Pacific during 1970–1991. *J. Climate*, **9**, 1840–1855.
- Giese, B. S., S. C. Urizan, and N. S. Fuckar, 2002: Southern Hemisphere origin of the 1976 climate shift. *Geophys. Res. Lett.*, **29**, 1014, doi:10.1029/2001GL013268.
- Gu, D., and S. G. H. Philander, 1997: Interdecadal climate fluctuations that depend on exchanges between the Tropics and extratropics. *Science*, **275**, 805–807.
- Huang, B., and Z. Liu, 1999: Pacific subtropical–tropical thermocline water exchange in the NCEP ocean model. *J. Geophys. Res.*, **104** (C5), 11 065–11 076.
- Johnson, G. C., and M. J. McPhaden, 1999: Interior pycnocline flow from the subtropical to equatorial Pacific Ocean. *J. Phys. Oceanogr.*, **29**, 3073–3089.
- Kleeman, R., J. P. McCreary, and B. A. Klinger, 1999: A mechanism for generating ENSO decadal variability. *Geophys. Res. Lett.*, **26**, 1743–1746.
- Levitus, S., 1982: *Climatological Atlas of the World Ocean*. NOAA Prof. Paper 13, 173 pp. and 17 microfiche.
- Liu, Z., 1996: Thermocline variability in different dynamical regimes. *J. Phys. Oceanogr.*, **26**, 1633–1645.
- , and J. Pedlosky, 1994: Thermocline forced by annual and decadal surface temperature variation. *J. Phys. Oceanogr.*, **24**, 587–608.
- , and R. H. Zhang, 1999: Propagation and mechanism of decadal upper-ocean variability in the North Pacific. *Geophys. Res. Lett.*, **26**, 739–742.
- , S. G. H. Philander, and R. C. Pacanowski, 1994: A GCM study of tropical–subtropical upper-ocean water exchange. *J. Phys. Oceanogr.*, **24**, 2606–2623.
- Lysne, J., P. Chang, and B. Giese, 1997: Impact of the extratropical Pacific on equatorial variability. *Geophys. Res. Lett.*, **24**, 2589–2592.
- McCreary, J., and P. Lu, 1994: On the interaction between the subtropical and the equatorial oceans: The subtropical cell. *J. Phys. Oceanogr.*, **24**, 466–497.
- , and —, 2001: Influence of the Indonesian Throughflow on the circulation of Pacific intermediate water. *J. Phys. Oceanogr.*, **31**, 932–942.
- McPhaden, M. J., and D. X. Zhang, 2002: Slowdown of the meridional overturning circulation in the upper Pacific Ocean. *Nature*, **415**, 603–608.
- Miller, A. J., D. R. Cayan, T. P. Barnett, N. E. Graham, and J. M. Oberhuber, 1994: Interdecadal variability of the Pacific Ocean: Model response to observed heat flux and wind stress anomalies. *Climate Dyn.*, **9**, 287–302.
- Nonaka, M., and S.-P. Xie, 2000: Propagation of North Pacific interdecadal subsurface temperature anomalies in an ocean GCM. *Geophys. Res. Lett.*, **27**, 3747–3750.
- , —, and K. Takeuchi, 2000: Equatorward spreading of a passive tracer with application to North Pacific interdecadal temperature variations. *J. Oceanogr.*, **56**, 173–183.
- , —, and J. P. McCreary, 2002: Decadal variations in the subtropical cells and equatorial Pacific SST. *Geophys. Res. Lett.*, **29**, 1116, doi:10.1029/2001GL013717.
- Pacanowski, R. C., and S. M. Griffies, 1999: *MOM 3.0 Manual*, NAA/Geophysical Fluid Dynamics Laboratory, 455 pp.
- Pierce, D., 1996: Reducing phase and amplitude errors in restoring boundary conditions. *J. Phys. Oceanogr.*, **26**, 1552–1560.
- , T. P. Barnett, and M. Latif, 2000: Connections between the Pacific Ocean Tropics and midlatitudes on decadal timescales. *J. Climate*, **13**, 1173–1194.
- Rothstein, L. M., R. H. Zhang, A. J. Busalacchi, and D. Chen, 1998: A numerical simulation of the mean water pathways in the subtropical and tropical Pacific Ocean. *J. Phys. Oceanogr.*, **28**, 322–343.
- Schneider, N., A. J. Miller, M. A. Alexander, and C. Deser, 1999a: Subduction of decadal North Pacific temperature anomalies: Observations and dynamics. *J. Phys. Oceanogr.*, **29**, 1056–1070.
- , S. Venzke, A. J. Miller, D. W. Pierce, T. P. Barnett, C. Deser, and M. Latif, 1999b: Pacific thermocline bridge revisited. *Geophys. Res. Lett.*, **26**, 1329–1332.
- Shin, S.-I., and Z. Liu, 2000: On the response of the equatorial thermocline to extratropical thermal forcing. *J. Phys. Oceanogr.*, **30**, 2883–2905.
- Stephens, M., Z. Liu, and H. Yang, 2001: Evolution of subduction planetary waves with application to North Pacific decadal thermocline variability. *J. Phys. Oceanogr.*, **31**, 1733–1745.
- White, W. B., 1995: Design of a global observing system for gyrescale upper ocean temperature variability. *Progress in Oceanography*, Vol. 36, Pergamon, 169–217.
- , and D. R. Cayan, 1998: Quasiperiodicity and global symmetries in interdecadal upper ocean temperature variability. *J. Geophys. Res.*, **103** (C10), 21 335–21 354.
- Xie, S.-P., T. Kunitani, A. Kubokawa, M. Nonaka, and S. Hosoda, 2000: Interdecadal thermocline variability in the North Pacific for 1958–97: A GCM simulation. *J. Phys. Oceanogr.*, **30**, 2798–2813.
- Zhang, R. H., L. M. Rothstein, and A. J. Busalacchi, 1998: Origin of warming and El Niño change on decadal scales in the tropical Pacific Ocean. *Nature*, **391**, 879–883.